Materials Today Advances 22 (2024) 100494

Contents lists available at ScienceDirect

Materials Today Advances

journal homepage: www.journals.elsevier.com/materials-today-advances/

In situ TEM investigation of nickel catalytic graphitization

Jaemin Kim [a,b], Seungwoo Son [b], Myeonggi Choe [a,b], Zonghoon Lee [a,b,*]

[a] Center for Multidimensional Carbon Materials, Institute for Basic Science (IBS), Ulsan 44919, Republic of Korea
[b] Department of Materials Science and Engineering, Ulsan National Institute of Science and Technology (UNIST), Ulsan 44919, Republic of Korea

ARTICLE INFO

Keywords:
In situ TEM
Graphene growth mechanism
Nickel catalyst
Solid carbon source
Graphitic layers

ABSTRACT

With the increasing demand for production of graphitic materials for various applications, it becomes crucial to get a fundamental understanding of how graphene layers grow on metal catalysts. Here, we performed an *in situ* heating transmission electron microscopy (TEM) study to understand the mechanism of graphitization of amorphous carbon (a-C) on Ni catalyst by following graphene growth at atomic resolution in real time. By discerning the Ni_3C phase from the pure Ni phase during the graphitic carbon growth process, we demonstrate that growth occurs through the carbide graphitization of Ni_3C. Additionally, during the graphitization, Ni diffusion has a crucial effect on the structure of the resulting graphene. Under our experimental conditions, we observed graphene contains islands of multilayers. Based on our *in situ* experimental results, we suggest a mechanism for graphitization of the a-C/Ni system and explain the dynamics resulting from Ni diffusion. Our study can contribute to the control of graphitization by using Ni catalyst in the production of graphene and other graphitic materials.

1. Introduction

Graphene is a single layer of carbon atoms arranged in a hexagonal lattice structure. It is the fundamental building block of all types of graphitic structures. Each carbon atom in graphene is bonded to three neighboring carbon atoms, forming a strong and stable two-dimensional sheet. Following the exfoliation of graphene from graphite by Geim et al., many studies have been reported describing the different methods of graphene manufacturing [1]. Currently, catalytic chemical vapor deposition (CVD) is the main method used to prepare graphene on the large scale [2]. Since the graphitization of a carbon precursor requires very high energy in the absence of a catalyst, different transition metals have been studied for their effectiveness as catalyst both to improve energy efficiency and to grow better quality graphene [3–5]. Due to its negligible solubility for carbon, Cu has been found to be an ideal catalyst for the growth of single layer graphene, whereas catalysts like Ni are advantageous for the growth of multilayer graphene due to their high C solubility. Graphitization on Ni is known to occur through a carbon (C) precipitation reaction of solute carbon in Ni during cooling [6–8]. However, some studies have proposed the formation of an intermediate carbide phase during the catalytic graphitization on Ni. In this mechanism, both Ni and C undergo phase transition to Ni carbide phase at temperatures below the reaction temperature. The carbide phase become unstable above 450 °C and decomposes to form Ni and C, following which, graphitization occurs by the catalytic effect of Ni [9–12].

Previous studies on catalytic growth of graphene have compared the efficacy of the different catalysts used and the morphology of the grown graphene for each of these catalysts. An aberration-corrected TEM allows to observe graphene at atomic resolution and the development of modern *in situ* TEM enables real time investigation of the intermediate processes during graphene formation. *In situ* TEM has been applied to measure graphene growth rate through a layer-by-layer growth reaction (J. Kling et al.) [13] or to study the effect of the catalyst size and shape on the morphology of the grown graphene (Z. Peng et al.) [14]. Since TEM analysis requires thin specimens to transmit the electron beam, *in situ* TEM observation is limited to nanoscale membranes or nanoparticles. When observing a nanoscale experimental system using TEM, the dynamic motion of the specimen may occur. This motion might perturb *in situ* analysis, but it also contains information related to the reaction kinetics. In the Ni nanosized catalyst system, normally graphene grows at the surface of the particle, but sometimes a Ni particle can migrate on the a-C film leaving behind a trail of graphene. R. Anton et al. demonstrated that graphene grows on the trace of Ni particles. Deactivated Ni particles can be reactivated and used to grow graphene by contacting activated Ni particles [15]. More recently, Y. Lyu et al.

* Corresponding author. Center for Multidimensional Carbon Materials, Institute for Basic Science (IBS), Ulsan 44919, Republic of Korea.
E-mail address: zhlee@unist.ac.kr (Z. Lee).

https://doi.org/10.1016/j.mtadv.2024.100494
Received 19 March 2024; Received in revised form 17 April 2024; Accepted 24 April 2024
Available online 13 May 2024

used *in situ* TEM to reveal that Ni particle showed synchronized oscillation of tip stretch and atomic step fluctuations in a cyclic manner during continuous graphitization [16].

In our *in situ* TEM growth system, Ni catalysts are utilized to grow graphene from a solid C source. The experiment is designed to focus on the Ni–C catalytic reaction, with Ni and C being the only input materials and heat being the only external stimulus. The high vacuum maintained by the TEM column ensures that only chemical compounds belonging to the Ni–C system are formed during the *in situ* TEM heating experiment. Thus, we used this experimental condition to investigate the mechanism of graphitic growth on Ni catalyst without the involvement of other sources.

For *in situ* heating TEM experiments, we sequentially deposited a-C and Ni thin films. The a-C/Ni film was placed at a hole to be freestanding and growth of graphene layers were performed by *in situ* heating under a high vacuum condition.

In this *in situ* study, we revealed the presence of an intermediate Ni_3C phase with a very slight lattice alteration of Ni. Using atomic resolution TEM real-time imaging, we elucidated the growth mechanism of graphene layers on Ni catalyst during heating. Additional analyses including X-ray energy dispersive spectroscopy (EDS) and electron energy loss spectroscopy (EELS) were carried out to ensure that the grown material was graphene layers. From the morphology of the grown graphene layers under different experimental conditions, we elucidated the intricate connection between the dynamic diffusion of Ni and the process of graphene growth during heating.

2. Experimental method

2.1. Specimen preparation

In this study, we used an a-C/Ni thin film (5/5 ± 0.5 nm thickness) deposited by sputter (Ni)/evaporator (a-C) (Leica, ACE 600). The thin film was deposited onto a rock salt substrate. With this rock salt transfer method, there is no need for any supporting layers for transfer and the substrate is easily and clearly removed from water. In this manner, any residues from preparation step can be avoided [17].

This film was transferred to MEMS device for *in situ* heating TEM experiments (DENSsolutions) by scooping the floated thin film in water.

2.2. In situ TEM experiment and analysis

We used the aberration-corrected TEM (Thermofisher, Titan^3 G2 60–300) for atomic resolution TEM/scanning transmission electron microscopy and *in situ* heating system (DENSsolutions, gas flow system for *in situ* TEM). The acceleration voltage was 80 kV with a monochromator to avoid knock-on damage on grown graphene. Graphitization started at 450 °C and hence the temperature as increased by 30 °C/min rate to 450 °C and monitored in dwelling state. For better reliability in analyzing experimental data, we applied simulations of diffraction pattern (CrystalMaker software) and high-resolution TEM images (TempasX software). Cross sectional specimens of as-deposited thin films and reference Ni_3C samples (Americanelements) were prepared by Quanta FIB (Thermofisher) for TEM analyses.

3. Results

3.1. In situ TEM observation of graphitization

Fig. 1 and supporting movie 1 show *in situ* growth of graphene layers on a-C/Ni thin film in TEM. The a-C/Ni film was prepared by a physical vapor deposition method and transferred onto an *in situ* heating device as shown in Fig. S1. The as-deposited Ni film has a nanocrystalline microstructure as shown in a cross-sectional image in Fig. 1b. During the heating of the film, below the growth temperature of 450 °C, carbon diffuses into the nickel lattice to form a nickel carbide. This step consists in the recrystallization and agglomeration of the Ni film without graphene growth. Above 450 °C, nickel carbide decarburized and the precipitated C grows in the form of graphene onto the Ni_3C surface (Fig. 1d). During graphene layers growth from the precipitated C, the agglomeration of Ni and nickel carbide decomposition continue, as revealed by the grown graphene layer (Fig. 1e).

From the *in situ* TEM results, we infer that Ni and Ni_3C phase coexist during growth of graphene layers. The atomic resolution TEM image in

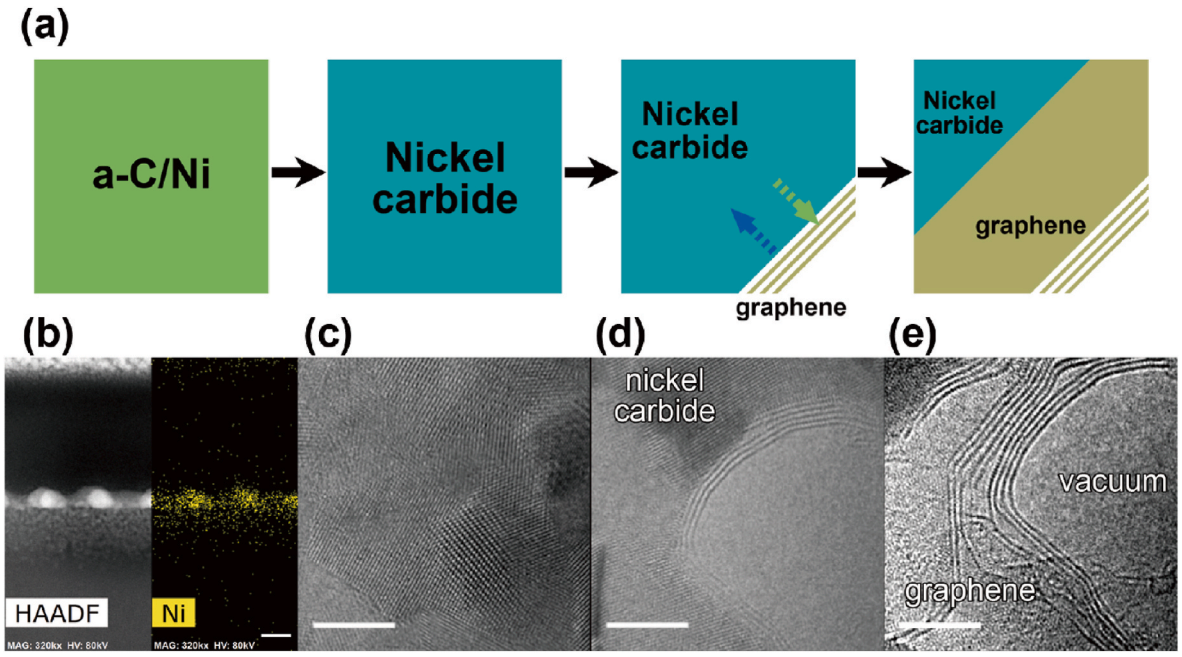

Fig. 1. (a) Schematics showing the change in the a-C/Ni film during *in situ* heating. (b) The cross-sectional STEM image and corresponding EDS map of as deposited Ni film onto the SiO_2, for the measuring of deposited film. (c–e) Fig. 1c–e are the capture from the *in situ* experiment. Fig. 1c is showing as reaching to 450 °C. Fig. 1d shows the image from 90 s later from c. Fig. 1e image showing after 120 s from Fig. 1d. The HRTEM images corresponding to the different stages captured from the supporting movie 1. (Scale bar in b = 20 nm, c–e = 5 nm).

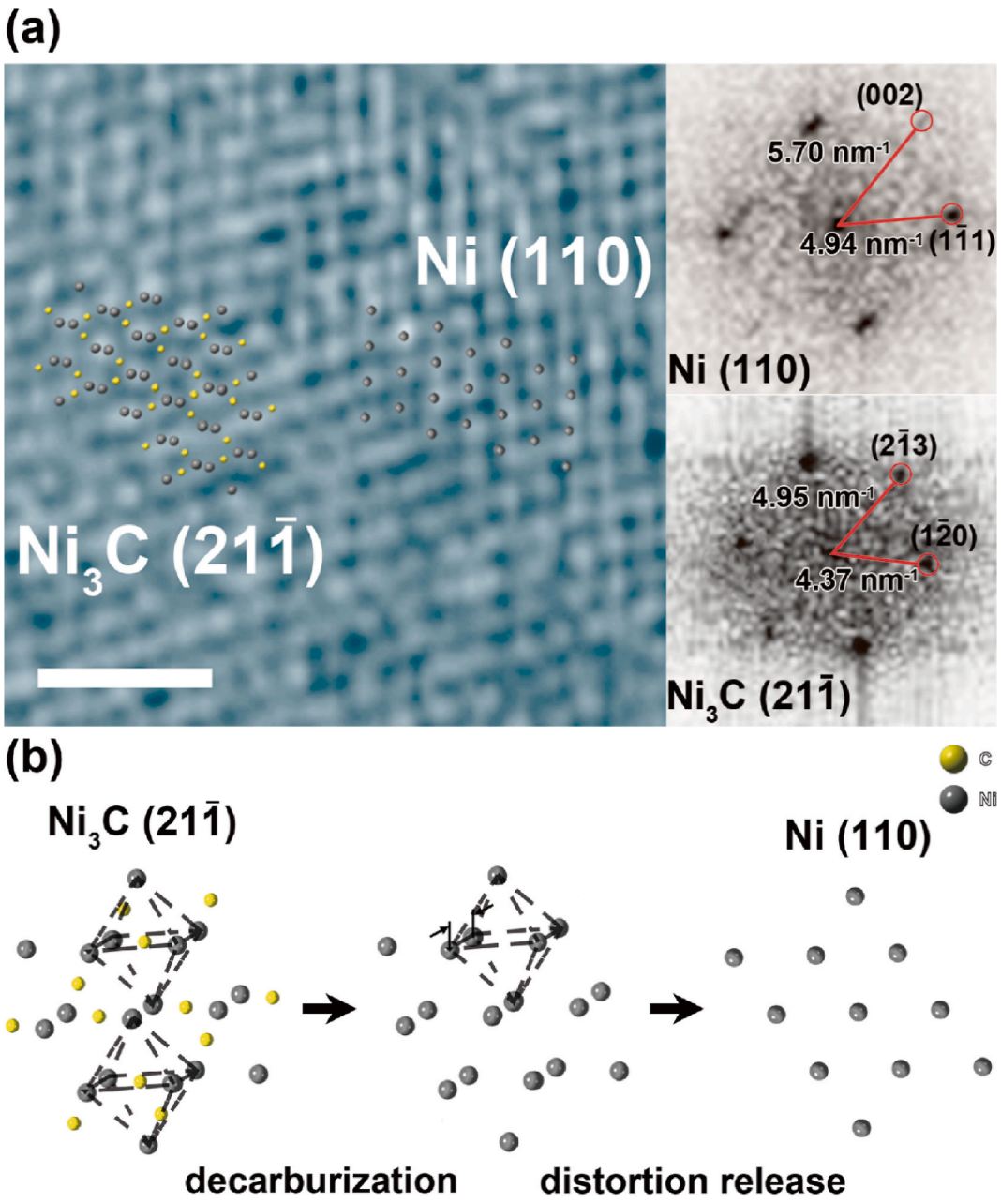

Fig. 2. (a) Atomic resolution image of the reaction surface. Ni and Ni_3C lattices are overlaid on the HRTEM image for clarity; the corresponding FFT of each phase is shown. The image is captured during the *in situ* TEM heating experiment at 450 °C. (Scale bar = 1 nm) (b) Phase transition by decarburization from Ni_3C (21$\bar{1}$) to Ni (110). Data retrieved from the Materials Project for Ni (mp-23) and Ni_3C (mp-7586) from database version v2022.10.28 [21].

Fig. 2a shows the coexisting Ni (110) and Ni_3C (21$\bar{1}$) phases with their atomic models overlaid. The Ni_3C carbide phase contains C atoms in the octahedral sites of the Ni crystal [18–20]. The presence of this C atom creates a lattice distortion of Ni as shown in Fig. S2. For this reason, it is difficult to distinguish Ni and Ni_3C using diffraction methods. In Fig. 2, we distinguish them by the atomic resolution TEM image and its Fast Fourier Transformation (FFT). In Fig. 2a, a well aligned zone axis in Ni (110) is seen at the area on the top right, while the left bottom area shows a slightly different lattice image. With the observed difference in d spacing (though small) and FFT, this area is identified to be Ni_3C (21$\bar{1}$) in Fig. 2a. We also show a reference sample data in the supporting information (Fig. S3). Both Ni(110) and Ni_3C(21$\bar{1}$) planes face the octahedral sites, as shown in Fig. 2b. From the TEM image, it can be observed that there is a difference in the spacing between the Ni atoms, which is consistent with the known spacing of pure Ni and Ni_3C. At 450 °C. a carbon atom occupying an octahedral site is removed from Ni_3C, which releases the lattice distortion of the remaining Ni lattice. Since the Ni_3C (21$\bar{1}$) plane is the result of a distortion of the Ni lattice, the octahedral Ni (110) lattice is restored upon C removal. The separated C atom diffuses to the surface and forms a graphene film at the surface and the Ni_3C surface thus forms a graphene/Ni/Ni_3C layered structure. Additional graphene layers are formed below the previous layers (so-called bottom growth) by carbon formed from the decarburization of the underlying Ni_3C. Under our experimental conditions, there is an excess of C (much above the stoichiometric level) but this excess C remains in the a-C film and does not function as a carbon supply, but plays the role of a substrate. At temperatures over 450 °C, Ni did not undergo transition to the carbide phase since this phase is metastable at these temperatures. Hence, the a-C film could not be consumed to form the carbide.

3.2. Graphitization process

Thus, in our *in situ* TEM experiments, we have directly imaged the graphene growth process. Images in Fig. 3a show the time-elapsed image of graphene growth extracted from the supporting movie 1. Interestingly, our system did not exhibit a layer-by-layer process for graphene growth. Instead, a few layers grew simultaneously as the surface Ni was removed as shown in Fig. 3. In Fig. 3c, the graphene growth was often paused in the region indicated by the white arrow and Ni was removed from the graphene layer. The growth resumed after a few seconds later, but a vacant region remained between the layers of graphene. The vacancy site formed during a growth pause is similar to a graphene (0001) plane revealed at the termination step. Both represent arrested graphene growth at the Ni edge. For vacancy formation, it was observed that graphene growth restarts at the same temperature after a few seconds. It implies that the pause in growth is not caused by a catalytic effect, but rather to a potential lack of carbon supply. It appears that the carbon supply was interrupted at that surface, which halted the growth of graphene. During graphitization, the carbon source comes from the decarburization of carbide [10]. Note that this process does not take into account the carbon diffusion from the a-C film, which plays a role in bottom growth. Fig. 3f and g describe the simultaneous growth of graphene with nickel removal on the surface. The images indicate that the outer Ni lattice was removed and replaced by a graphene layer. The schematic on Fig. 3h illustrates the replacement of the Ni surface with graphene. It is suggested that the growth of the graphene layer tends to follow the morphology of the Ni on the imaging. As a result, a vacant region can be observed without the need for any mechanical force, but rather due to Ni delamination. Since the growth occurred at a comparatively low temperature, the removed nickel atoms are expected to diffuse out from the surface, not sublimation. but this diffusion path could not be ascertained from our *in situ* TEM imaging.

3.3. Structural analysis of grown graphitic film

At the growth termination step, while Ni/Ni_3C diffused out, this allowed to reveal the graphene plane as shown in Fig. 4. The diffraction pattern from the revealed area shows a hexagonal pattern which indicates d spacing of graphene. Fig. 4b shows planview HRTEM images on the marked region on Fig. 4a. In addition, electron energy loss spectroscopy (EELS) from this region shows sharp π* (~285 eV) and σ* (~292 eV) peaks characteristic of graphene (Fig. 4c). The FFT pattern from this region and the diffraction pattern have the same main hexagonal pattern, but on the FFT, other weak patterns are seen (Fig. 4a and b inset). These weak patterns in the FFT point to the presence of different nanograins of graphene on the graphene film, as confirmed from the moiré pattern on the HRTEM images. For example, graphene moiré patterns with a rotation of 20° are seen in Fig. 4b. We have overlaid on the image, the result from image simulation of a 20°-rotated graphene stacked on graphene for better clarity. The simulation and the real HRTEM image nearly match, but some contrast inversions are present, due to different defocus. In addition, HRTEM images of graphene grown from our *ex situ* experiments under the same condition are given in Fig. S4 for comparison. The microstructure of graphene layers from *ex situ* experiments conducted under the same conditions is comparable to that of *in situ* counterparts. The images represent turbostratic graphene multilayers. The blurred regions in the HRTEM images are due to the fact that the grown graphitic film is not perfectly flat for HRTEM

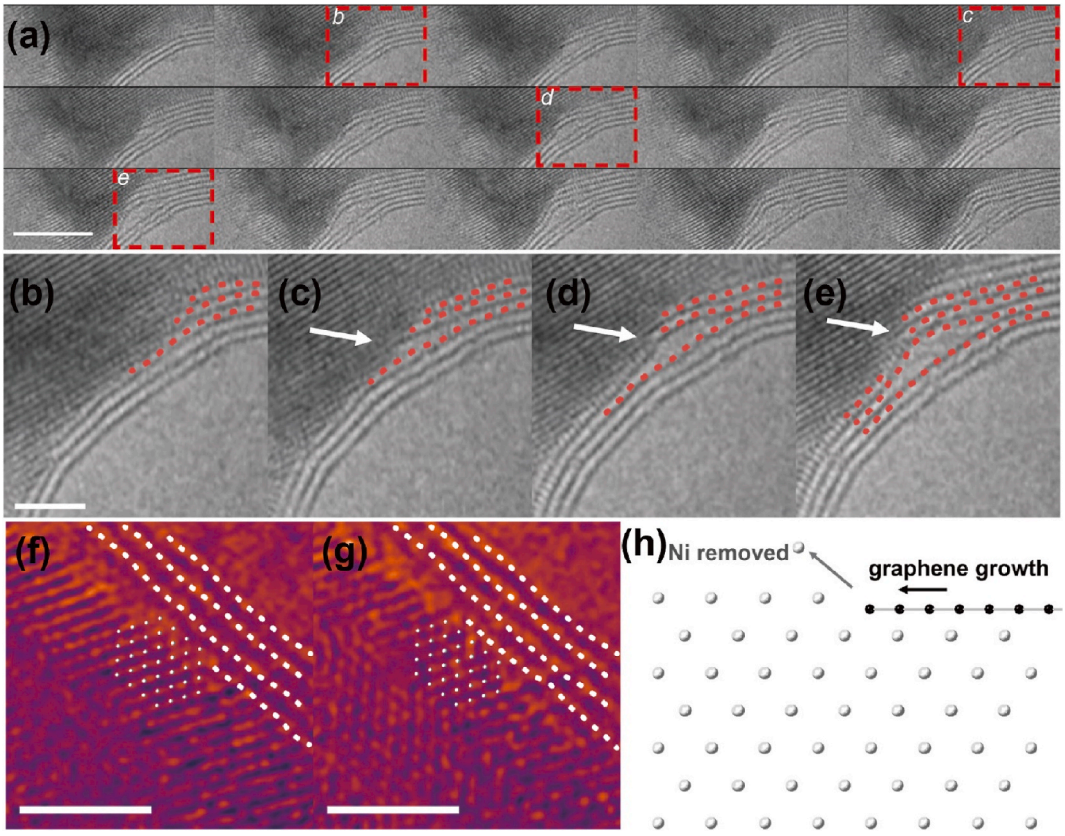

Fig. 3. (a) Growth process of graphene layers at the Ni surface in 1 s interval time-elapsed images. Four selected images marked with the red dotted boxes are shown in enlarged images of b-e with the indication of grown graphitic layers near catalyst, respectively. (f–g) Atomic scale graphitization process with removal of Ni. The smaller white dot pattern overlaid on the image is the Ni (110) lattice, and the white dotted lines are the grown graphene layers. (h) Schematics of graphitization with Ni removal (Scale bar = 2 nm). Data retrieved from the Materials Project for Ni (mp-23) from database version v2022.10.28. (For interpretation of the references to colour in this figure legend, the reader is referred to the Web version of this article.)

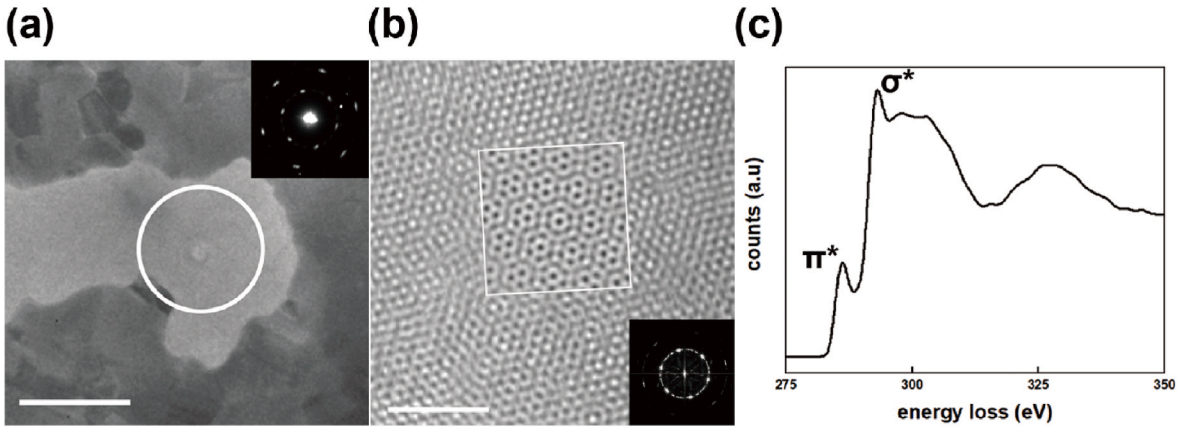

Fig. 4. (a) A low magnification TEM image of the sample after *in situ* heating (inset diffraction pattern was acquired from the white circle area). (b) A planview HRTEM image from the marked area on (a) and its FFT in inset. Corresponding image simulation with white box overlayed on the HRTEM image. (c) Electron energy loss spectroscopy (EELS) of the grown graphene. (scale bar on a = 100 nm, b = 2 nm).

imaging.

Analysis of the grown graphene film through *in situ* experiments shows a rough surface including multilayer graphene overlaid on the graphene plane. Fig. 5a and b and supporting movie 2 show a layered graphene growth onto the graphene plane. The growth process is similar to the growth at the initiation step, but there is no thickness change in the in-plane direction, as shown by the line profile in Fig. 5C measured along the path shown by the black arrow on Fig. 5b. The line profile and the image have almost similar intensity both at the end and at the start points, irrespective of whether additional layers were present or not. The layered graphene grows 17 layers which is in accordance with the line profile. If the initially grown graphene plane also grew 17 additional layers, there should be a significant change in contrast in TEM imaging. As an example, Fig. S5 shows an HRTEM image from the stacked graphene layers grown by *ex situ* condition, which demonstrate change in the thickness contrast in TEM. However, both initial, terminating and in-between layers have the same contrast, indicating that these vertical layers grow along the lateral direction with no thickness change. In the supporting movie 2, we present that the Ni-catalyzed graphene growth occurred in such a way that vertical multilayer were subsequently grown on graphene plane.

From the above analysis, we conclude that the graphene grown in our experiments has a three-dimensional (3D) structure including multilayers of graphene forming islands on a graphene plane. While it is

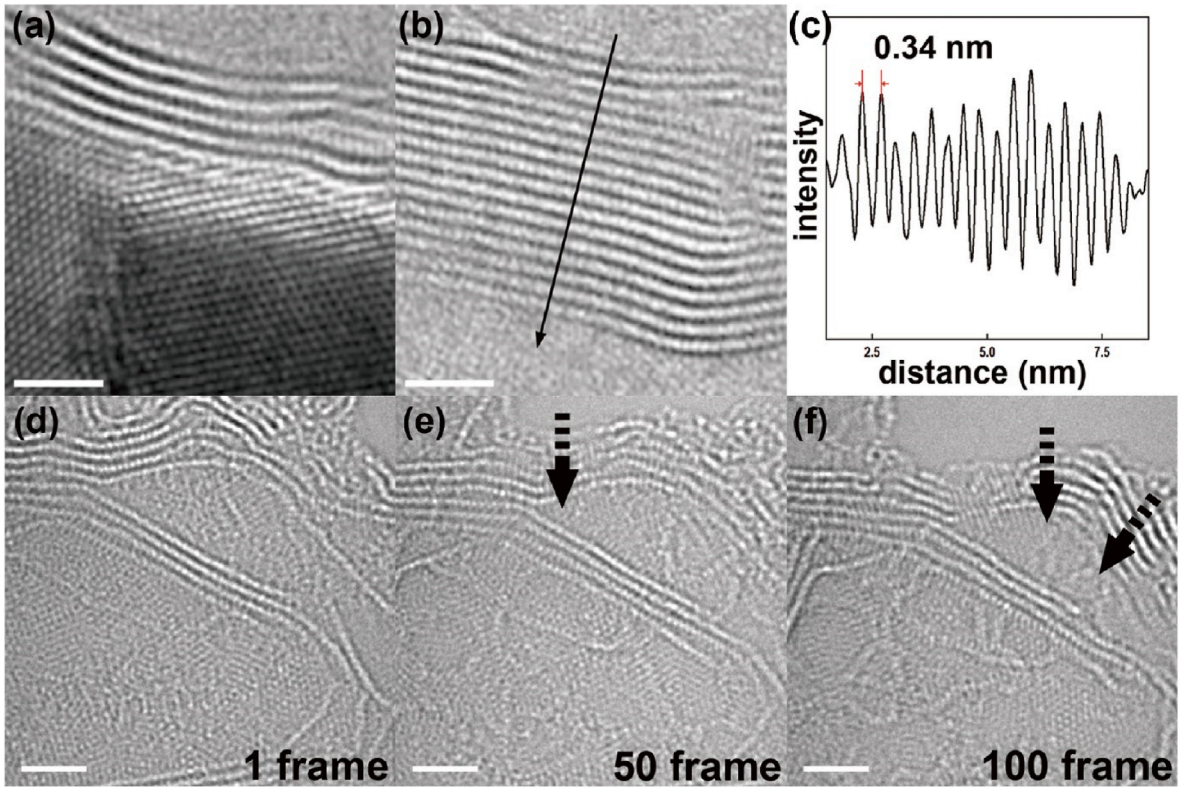

Fig. 5. (a), (b) Vertical graphene growth along the (0001) direction at 450 °C during *in situ* heating, and (c) a line profile of contrast along the arrows in (b). (d) To (f) show a sequential electron beam etching of the edge of the grown graphene with time at room temperature with 80 keV electron beam irradiation captured by time series. The images are acquired from the first, middle, and last frame of the time series. The arrows show the direction of crumbling of the graphene film from the edge. (scale bar = 2 nm).

clearly seen that graphene growth occurs at the Ni/Ni_3C surface, but it cannot be verified whether graphene also grows at the a-C interface. Electron beam etching was applied to further characterize the 3D morphology of our graphene. We designed our experiment to retain excess a-C film on the top which works as a substrate on the freestanding system. Since the a-C film is less stable than pristine graphene to electron beam, following electron beam etching at the edge, the graphene layers moved and crumbled. Fig. 5d to f and supporting movie 3 show the time series images of electron beam etching. When the a-C was etched, the edge of the grown graphene crumbled (in the direction of the arrow on Fig. 5e and f). This part shows the grown graphitic layer morphology with the electron beam irradiation. Our beam irradiation experiment revealed that graphitization occurred at the surface of Ni but not at the a-C/Ni interface. The morphology can also be explained by the differences in interface energy. As graphitization progressed, the interface energy decreased. Therefore, it is important to determine which interface (surface) has a higher energy in our system. Previous studies reported that Ni has a higher surface energy of about 2 eV. Therefore, the graphitization process should aim to reduce the Ni surface rather than the a-C/Ni interface [22,23].

4. Discussion

Based on the our *in situ* TEM study, we propose a mechanism for graphene growth in the a-C/Ni system. Below the growth temperature of 450 °C, phase transition of Ni and C to Ni_3C occurred. In our experimental condition, we deposited an excess of carbon compared to Ni_3C. As shown in Fig. 6, there is a portion of the a-C film remaining at the top, which functions as a substrate. Above 450 °C, Ni_3C decomposed to Ni and C and the C from Ni_3C grew graphene by a catalytic reaction with Ni. In the graphene growth step, Ni out diffusion occurred as shown in Figs. 2 and 3. Thus a graphene/Ni/Ni_3C layered structure was formed as schematically shown in Fig. 6. The out diffusion of Ni caused a gradient in the thickness of Ni layer. The thickness of the Ni layer increased, except at the surface where graphene grew. This occurred due to the decarburization of the carbide and diffusion from the growth surface as indicated by the blue arrows. Interestingly, we observed that graphene growth was terminated in the region with high Ni thickness. In our system, all the carbon for graphene growth was supplied by the Ni_3C layer, since no carbon was supplied from the a-C film. If the Ni layer becomes too thick, it is difficult for carbon to penetrate through it, as suggested from molecule dynamic simulation on Ni_3C from Jiao et al. [20] Thus the selective graphene growth in the vertical direction along the (0001) takes place, similar to depicted in Fig. 5 and supporting movie 2.

In our study, we directly observed the growth of graphene in a-C/Ni thin film through the Ni_3C phase. However, some studies have suggested the presence of another carbide phase, Ni_2C, which is known as a surface-confined carbide phase for Ni. This phase has a similar graphene growth temperature to the Ni_3C phase, as shown by Rameshan et al. and Patera et al. [24,25]. Patera et al. demonstrated the surface-confined structure of Ni_2C and its graphene growth process using *in situ* STM. They identified two different modes of graphene growth on Ni_2C: on the surface and through replacement of Ni_2C. Our *in situ* TEM results, including Ni_3C (Fig. 3) [25], are consistent with the latter mode. The difference between Ni_3C and Ni_2C is suggested by the different C precursor state. With a solid C precursor, the carburization of Ni was directed towards the Ni_3C phase, as in our experiment. However, when using a gas C precursor such as ethylene, the carburization was directed towards Ni_2C phases, as reported by Martinez-Gordillo R. et al. [26].

Regarding the Ni diffusion path, we suppose that the diffusion of Ni occurred through the graphene/Ni interface. Confirmation that graphene did not grow at the a-C interface was obtained through an etching experiment on the grown graphene, as shown in Fig. 5. Other studies which have used a-C as a C precursor on Ni catalysts have also shown that graphene did not grow at the a-C interface [5,7,27]. Therefore, there are two pathways for Ni diffusion, namely, the a-C/Ni_3C interface, or the graphene/Ni interface. Previous studies have shown that Ni atom has high mobility at graphene interfaces [28,29]. Combining this observation with the selective growth results as illustrated in Fig. 6, we conclude that Ni diffused at the interface with graphene. Along this diffusion path, Ni atoms diffusing from the graphene interface have the effect of making the Ni layer thicker, which blocks the C supply from the carbide. Due to this effect, graphene growth takes place exclusively at the thin Ni/Ni_3C surface. The vacancy between the graphene planes, as shown in Fig. 3, may have the same origin, but in this case, there is a brief interruption in the supply of C, which is quickly restored. At the termination step, Ni flow at the Ni/Ni_3C surface reaches an equilibrium state in such a way that the C from the carbide cannot penetrate through the Ni layer.

Based on these results, we propose a graphene growth mechanism on our a-C/Ni system as shown schematically in Fig. 6. Above the growth temperature, Ni_3C decarburized from the surface region. The separated Ni and C functioned as the catalyst and carbon precursor, respectively. As demonstrated earlier, the a-C film itself did not participate in graphene growth. The Ni_3C phase is metastable and becomes unstable at

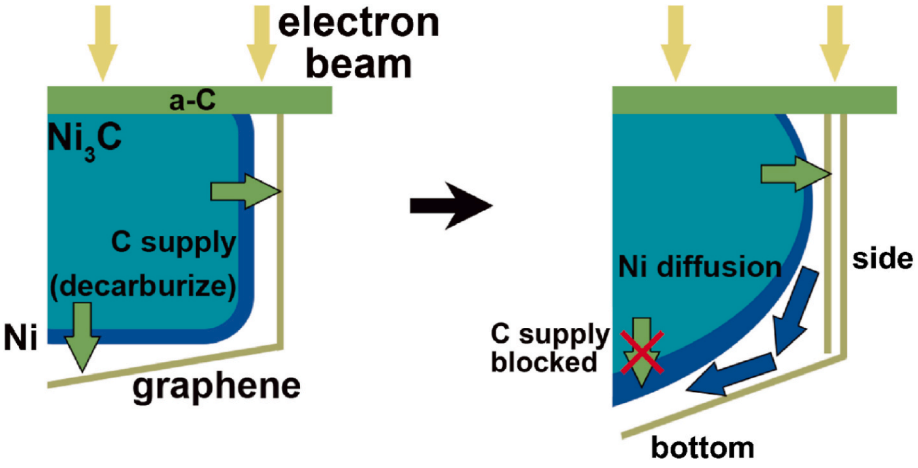

Fig. 6. Schematics of the graphene growth process based on *in situ* TEM observations. Carbon for the graphene growth is supplied from decarburization of Ni_3C and the formed graphene/Ni/Ni_3C layered structure. Thermal diffusion of Ni may occur from the side as shown by the arrow. During diffusion, the Ni layer has a thickness gradient that is thin at the side and thicker at the bottom along the diffusion path of Ni. This results in the selective growth of graphene as illustrated in the schematic. In addition, we also conclude that graphene did not grow at the a-C interface.

growth temperatures above 450 °C. Thus, additional carbide phase did not form during graphene growth. Moreover, since the carbon from a-C is not directly supplied to Ni, the a-C film remains intact after graphene growth in the form of a substrate as shown in Fig. 6. Graphene layers grow on the Ni surface, during which time Ni diffuses from the growth surface, and the diffusion of Ni occurs through the graphene/Ni interface as schematically illustrated in Fig. 6. The C supplied from the carbide phase should then penetrate the Ni layers to reach surface, but if the Ni layer becomes too thick, graphene growth terminates in that area due to the lack of precursor supply. In our system, Ni diffusion through graphene interface resulted in a thickness gradient between the top surface and the bottom of the film. Since the C supply was blocked at the graphene interface due to the thick Ni layer, the graphene grows only at the side, and not on the (0001) plane. As a result, graphene grows with a hemisphere morphology except at the interface with a-C.

5. Conclusion

In this study, we designed an *in situ* TEM graphene growth experiment using Ni and solid a-C to reveal the graphene growth mechanism on Ni catalyst. Below the growth temperature, Ni and C undergo a phase transition to the Ni_3C phase. In this phase, C atoms occupy the octahedral sites of Ni. When compared to pure Ni, the spacing between the Ni atoms is slightly increased. At temperatures above 450 °C, Ni_3C is decarburized to form Ni and C. In this step, C grows in the form of graphene layers by catalytic effect of Ni. Since graphene growth coincided with Ni diffusion, the morphology of the grown graphene layers is strongly affected by the dynamics Ni diffusion, resulting in a 3D morphology. Analyzing the morphology of the grown graphene allowed to also understand the Ni diffusion dynamics since both these effects are strongly interdependent. Based on our *in situ* TEM experimental observations, we propose a growth mechanism of graphene layers in the a-C/Ni system. The findings of our study will greatly contribute to the control of graphitization from a solid source of carbon through the utilization of Ni catalysts in the production of graphene and other graphitic carbon.

Availability of data and materials

All data generated or analyzed during this study are included in this published article and its supplementary information files.

Funding

This work was supported by the Institute for Basic Science (IBS).

CRediT authorship contribution statement

Jaemin Kim: Writing – review & editing, Writing – original draft, Visualization, Methodology, Investigation, Formal analysis, Data curation, Conceptualization. **Seungwoo Son:** Methodology, Conceptualization. **Myeonggi Choe:** Visualization, Data curation. **Zonghoon Lee:** Writing – review & editing, Supervision, Resources, Project administration, Investigation, Funding acquisition, Data curation, Conceptualization.

Declaration of competing interest

The authors declare that they have no known competing financial interests or personal relationships that could have appeared to influence the work reported in this paper.

Data availability

Data will be made available on request.

Acknowledgements

This work was supported by the Institute for Basic Science (IBS-R019-G1).

Appendix A. Supplementary data

Supplementary data to this article can be found online at https://doi.org/10.1016/j.mtadv.2024.100494.

List of abbreviations

(TEM) Transmission electron microscopy
(HRTEM) High resolution transmission electron microscopy
(STEM) Scanning transmission electron microscopy
(EELS) Electron energy loss spectroscopy
(EDS) X-ray energy dispersive spectroscopy

References

[1] A.K. Geim, K.S. Novoselov, Nat. Mater. 6 (2007) 183–191, https://doi.org/10.1038/nmat1849.
[2] R. Muñoz, C. Gómez-Aleixandre, Chem. Vap. Depos. 19 (2013) 297–322, https://doi.org/10.1002/cvde.201300051.
[3] A. Barreiro, F. Börrnert, S.M. Avdoshenko, B. Rellinghaus, G. Cuniberti, M. H. Rümmeli, L.M.K. Vandersypen, Sci. Rep. 3 (2013), https://doi.org/10.1038/srep01115.
[4] J.A. Rodriguez-Manzo, C. Pham-Huu, F. Banhart, ACS Nano 5 (2011) 1529–1534, https://doi.org/10.1021/nn103456z.
[5] Y. Nakajima, H. Murata, N. Saitoh, N. Yoshizawa, T. Suemasu, K. Toko, ACS Appl. Mater. Interfaces 10 (2018) 41664–41669, https://doi.org/10.1021/acsami.8b14960.
[6] M. Losurdo, M.M. Giangregorio, P. Capezzuto, G. Bruno, Phys. Chem. Chem. Phys. 13 (2011) 20836–20843, https://doi.org/10.1039/c1cp22347j.
[7] L. Lu, J.T.M. De Hosson, Y. Pei, Mater. Des. 144 (2018) 245–255, https://doi.org/10.1016/j.matdes.2018.02.034.
[8] M. Huang, P.V. Bakharev, Z.J. Wang, M. Biswal, Z. Yang, S. Jin, B. Wang, H.J. Park, Y. Li, D. Qu, Y. Kwon, X. Chen, S.H. Lee, M.G. Willinger, W.J. Yoo, Z. Lee, R. S. Ruoff, Nat. Nanotechnol. 15 (2020) 289–295, https://doi.org/10.1038/s41565-019-0622-8.
[9] B.C. Bayer, D.A. Bosworth, F.B. Michaelis, R. Blume, G. Habler, R. Abart, R. S. Weatherup, P.R. Kidambi, J.J. Baumberg, A. Knop-Gericke, R. Schloegl, C. Baehtz, Z.H. Barber, J.C. Meyer, S. Hofmann, J Phys Chem C Nanomater Interfaces 120 (2016) 22571–22584, https://doi.org/10.1021/acs.jpcc.6b01555.
[10] W. Xiong, Y.S. Zhou, W.J. Hou, T. Guillemet, J.F. Silvain, Y. Gao, M. Lahaye, E. Lebraud, S. Xu, X.W. Wang, D.A. Cullen, K.L. More, L. Jiang, Y.F. Lu, RSC Adv. 5 (2015) 99037–99043, https://doi.org/10.1039/c5ra18682j.
[11] J. Han, G. Huang, Z. Wang, Z. Lu, J. Du, H. Kashani, M. Chen, Adv. Mater. 30 (2018) e1803588, https://doi.org/10.1002/adma.201803588.
[12] E.V. Zhizhin, D.A. Pudikov, A.G. Rybkin, A.E. Petukhov, Y.M. Zhukov, A.M. Shikin, Mater. Des. 104 (2016) 284–291, https://doi.org/10.1016/j.matdes.2016.04.091.
[13] J. Kling, T.W. Hansen, J.B. Wagner, Carbon 99 (2016) 261–266, https://doi.org/10.1016/j.carbon.2015.11.056.
[14] Z. Peng, F. Somodi, S. Helveg, C. Kisielowski, P. Specht, A.T. Bell, J. Catal. 286 (2012) 22–29, https://doi.org/10.1016/j.jcat.2011.10.008.
[15] R. Anton, Carbon 46 (2008) 656–662, https://doi.org/10.1016/j.carbon.2008.01.021.
[16] Y. Lyu, P. Wang, D. Liu, F. Zhang, T.P. Senftle, G. Zhang, Z. Zhang, J. Wang, W. Liu, Small Methods 6 (2022) e2200235, https://doi.org/10.1002/smtd.202200235.
[17] J. Yoon, Y. Jang, K. Kim, J. Kim, S. Son, Z. Lee, Carbon 196 (2022) 236–242, https://doi.org/10.1016/j.carbon.2022.04.062.
[18] Y. Ohta, Y. Okamoto, A.J. Page, S. Irle, K. Morokuma, ACS Nano 3 (2009) 3413–3420, https://doi.org/10.1021/nn900784f.
[19] N.E. Sagatov, A.U. Abuova, D.N. Sagatova, P.N. Gavryushkin, F.U. Abuova, K. D. Litasov, RSC Adv. 11 (2021) 33781–33787, https://doi.org/10.1039/d1ra06160g.
[20] M. Jiao, K. Li, W. Guan, Y. Wang, Z. Wu, A. Page, K. Morokuma, Sci. Rep. 5 (2015) 12091, https://doi.org/10.1038/srep12091.
[21] A. Jain, S.P. Ong, G. Hautier, W. Chen, W.D. Richards, S. Dacek, S. Cholia, D. Gunter, D. Skinner, G. Ceder, K.A. Persson, Apl. Mater. 1 (2013) 011002, https://doi.org/10.1063/1.4812323.
[22] Y. Chen, J. Wang, P. Schützendübe, Z. Wang, E.J. Mittemeijer, Carbon 159 (2020) 37–44, https://doi.org/10.1016/j.carbon.2019.12.017.
[23] D. Janke, F. Munnik, J. Julin, R. Hübner, J. Grenzer, C. Wüstefeld, S. Gemming, D. Rafaja, M. Krause, Carbon 159 (2020) 656–667, https://doi.org/10.1016/j.carbon.2019.12.006.
[24] R. Rameshan, V. Vonk, D. Franz, J. Drnec, S. Penner, A. Garhofer, F. Mittendorfer, A. Stierle, B. Klotzer, Sci. Rep. 8 (2018) 2662, https://doi.org/10.1038/s41598-018-20777-4.

[25] L.L. Patera, C. Africh, R.S. Weatherup, R. Blume, S. Bhardwaj, C. Castellarin-Cudia, A. Knop-Gericke, R. Schloegl, G. Comelli, S. Hofmann, C. Cepek, ACS Nano 7 (2013) 7901–7912, https://doi.org/10.1021/nn402927q.
[26] R. Martinez-Gordillo, C. Varvenne, H. Amara, C. Bichara, Phys. Rev. B 97 (2018), https://doi.org/10.1103/PhysRevB.97.205431.
[27] X. Li, Y. Zhou, X. Xu, A. Wang, K.R. Lee, Phys. Chem. Chem. Phys. 21 (2019) 9384–9390, https://doi.org/10.1039/c9cp01305a.
[28] Z. Lu, X. Sun, Y. Xiang, G.-C. Wang, M.A. Washington, T.-M. Lu, CrystEngComm 22 (2020) 119–129, https://doi.org/10.1039/c9ce01515a.
[29] Y. Yang, M. Liu, J. Du, W. Zhang, S. Zhou, W. Ren, Q. Zhou, L. Shi, Carbon 191 (2022) 55–66, https://doi.org/10.1016/j.carbon.2022.01.044.